ACS OMEGA

Open Access

http://pubs.acs.org/journal/acsodf

Article

Release of Crystalline Silica Nanoparticles during Engineered Stone Fabrication

Kabir Rishi, Bon Ki Ku,* Chaolong Qi, Drew Thompson, Chen Wang, Alan Dozier, Vasileia Vogiazi, Orthodoxia Zervaki, and Pramod Kulkarni

Cite This: *ACS Omega* 2024, 9, 50308−50317

Read Online

ACCESS | Metrics & More | Article Recommendations | Supporting Information

ABSTRACT: Inhalation exposure to respirable crystalline silica (RCS) during the fabrication of engineered stone-based kitchen countertops has been on the rise in recent years and has become a significant occupational health problem in the United States and globally. Little is known about the presence of nanocrystalline silica (NCS), i.e., particles below 100 nm. We present a methodology to quantify the crystalline silica content in the sub-100 nm size fraction of the aerosol released during engineered stone fabrication using X-ray diffraction (XRD) and Fourier transform infrared (FTIR) spectroscopy. Aerosol was generated in a test chamber designed per EN 1093-3 and sampled using cascade impactors. XRD and FTIR analysis showed the presence of both α-quartz (15−60%) and cristobalite (10−50%) polymorphs in all size fractions. With increasing particle size, the cristobalite content increased. Seventy percent of the total aerosol mass in the sub-100 nm fraction was found to be crystalline silica, qualitatively confirmed by electron diffraction and electron energy loss spectroscopy. The presence of other minerals was detected in all size fractions; no polymeric resin binder was detected in the sub-100 nm fraction. Although the sub-100 nm fraction was about 1% of the aerosol mass, it accounted for 4−24% of the aerosol surface area based on the total lung deposition. If the surface area is a more relevant exposure metric, the assessment of the efficacy of current engineering control systems using mass as an exposure metric may not provide adequate protection.

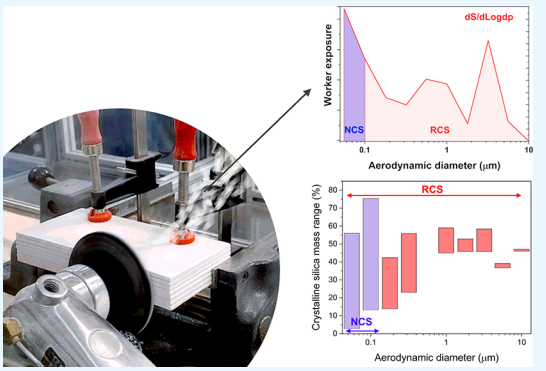

1. INTRODUCTION

Exposure to aerosol containing crystalline silica occurs during different construction activities.[1−6] Respirable crystalline silica (RCS) in the form of fractured particles produced by work activities such as cutting, breaking, crushing, drilling, or grinding of construction materials (i.e., rock, brick, concrete and engineered stone materials) is a significant occupational health problem in the United States. Inhalation of RCS can cause silicosis, lung cancer, and chronic obstructive pulmonary disease (COPD).[7−11] From the year 1990 to 1999, about 500 silicosis related deaths were reported in the construction and manufacturing sector in the U.S.[12]

The increasing popularity of engineered stone countertops among consumers has been evidenced by a 800% increase in U.S. imports between 2010 and 2018.[9] The U.S. stone fabrication industry employed 96,366 workers across 8,694 establishments as of 2018.[8] Silicosis has been identified among engineered stone workers in the U.S., Australia, Spain, and Israel.[8,13−21] Without validated engineering controls that include effective wetting methods and local exhaust ventilation to reduce the aerosol release at its source, the RCS exposure levels during grinding activity often exceed the permissible exposure limit of 50 $\mu g/m^3$ as an 8 h time-weighted average set by the Occupational Safety and Health Administration in the U.S.[22−26]

The release of RCS during grinding of stone countertops has been reported extensively.[23−25,27,28] While the characteristics of RCS inhalation exposure[11,29] and toxicity[30,31] are well documented, little is known about the presence of crystalline silica content in the sub-100 nm fraction, referred to as the nanocrystalline silica (NCS) here. Nanoparticles have shown to cause greater inflammatory responses and lung diseases than micron-sized particles per given mass,[32−34] although the relative toxicity of NCS compared to RCS was attributed to their surface activity based on the hemolytic potential.[35] While there is a plethora of studies on the pulmonary toxicity of nano- and micron-sized amorphous silica, NCS studies are sparse.[31] NCS, a subfraction of RCS, may pose greater health risks compared to coarse or fine silica particles due to their

Received: July 11, 2024
Revised: November 19, 2024
Accepted: November 26, 2024
Published: December 10, 2024

Table 1. Details of Generation, Sampling, Redeposition, and Analysis Methods for Engineered Stone Aerosol from Grinding and Calibration Samples

material	generation method	sampling method[a]	redeposition[b]	replicates	analysis method
engineered stone	grinding	MOUDI with PVC filter[c]		4	FT-IR[g]
		MOUDI with aluminum foil[d]	silver filter[e]	1	XRD,[g] O-PTIR[j]
		MOUDI	SEM stubs,[h] TEM grids[i]	1	SEM, TEM
SRM 1878	nebulization (aqueous)	QCM	silver filter[e]	1	XRD
SRM 1878b	vortex shaking (dry)[46]	MOUDI	PVC filter[f]	2	FT-IR
Min-U-Sil 5		MOUDI	silver filter[e]	1	XRD
		MOUDI with PVC filter[c]		1	FT-IR
		AAC	PVC filter[f]	1	
SRM 1879b		MOUDI	silver filter[e]	3	XRD
		MOUDI with PVC filter[c]		1	FT-IR
		MOUDI	PVC filter[f]	2	FT-IR

[a]If specified, filter/foil was mounted on the impactor substrates, else aerosol was sampled directly on the impactor substrates. [b]Substrates with sampled aerosol were rinsed in 2-propanol (A461−212, Optima LC/MS grade, Fisher Scientific). The resuspensions were vacuum filtered on the filtration media. [c]47 mm, 5 μm pore size, SKC, Inc. [d]47 mm, TSI Inc. [e]25 mm, 0.45 μm pore, SKC, Inc. [f]25 mm, pore size 5 μm, SKC Inc. The deposition area on these filters was smaller than the 47 mm PVC filters used for collecting the aerosol from grinding. For calibration, this difference was accounted for by normalizing the mass with the ratio of the deposition areas. [g]Mass of the sub-100 nm and submicron sized samples was much lower than the micron-sized samples. To minimize the potential particle loss during ashing when sampled on PVC filters as recommended in the NIOSH 7500[47] and NIOSH 7603[48] methods, we opted to resuspend the sampled aerosol on aluminum foil in 2-propanol and redeposit on silver filters for XRD. Additionally, we opted to measure the aerosol sampled on PVC filters directly for FT-IR. [h]Transferred to adhesive carbon conductive tabs (PELCO Image Tabs, Ted Pella, Inc.) mounted on SEM pin stubs (Aluminum, grooved edge, Ted Pella, Inc.) before rinsing the substrate in 2-propanol. [i]Sub-100 nm and submicron sized samples suspended in 2-propanol were pipetted onto TEM grids (400 mesh carbon coated Ni or Cu, SPI) and dried under ambient conditions. Micron-sized samples (dry collection) were transferred to the TEM grids using a needle-tip. [j]Measurements were performed on the same silver filters used for XRD.

higher specific surface area (surface area per unit mass) which could potentially result in greater toxicity.[36−38] Nanoparticles have a larger probability of being retained in the alveolar region compared to micron-size particles.[39−41] Nanoparticles also have longer settling times and therefore can persist longer in the workplace atmospheres, compared to micron-sized particles. However, analytical quantification of crystalline content in the sub-100 nm fraction has been challenging due to significantly low mass of crystalline silica and the very low detection limits required. Calibration for X-ray diffraction (XRD) and Fourier transform Infrared (FT-IR) methods for sub-100 nm fraction can be also challenging as the standard reference materials required for calibration are applicable only to the respirable size range.

The objective of this study was to quantify the size-resolved crystalline silica content in the sub-100 nm and respirable size factions of the aerosol released during the grinding of engineered stone. Different particle size fractions were collected using cascade impactors in the 0.056−10 μm range and analyzed using XRD and FT-IR methods. Calibration curves for different size fractions were developed for both methods. The morphology, chemical composition, and crystallinity of the aerosol were characterized using electron microscopy, spectroscopy, and diffraction techniques. Fractional silica content in various impactor stages is presented and discussed.

2. MATERIALS AND METHODS

2.1. Materials. A commercially available engineered stone was used for this study. According to the safety data sheet (SDS), this engineered stone was predominantly comprised of crystalline silica (>70% by mass) in a resin matrix with additives such as pigments and other minerals.

Crystalline silica content in the aerosol from grinding this engineered stone was quantified with reference to standard reference materials (SRM). In XRD and FT-IR methods, the α-quartz calibration plots were generated using SRM 1878 (National Institute of Standards and Technology, NIST), SRM 1878b (NIST), and Min-U-Sil 5 (US Silica Company, Berkeley Springs, WV) whereas SRM 1879b (NIST) was used for the cristobalite calibration.

2.2. Sample Collection. The experimental setup and test chamber shown in Figure S1 in the SI was designed for characterizing the generation rate of aerosol from various workplace tasks per the European Standard EN 1093−3.[42] This chamber was used in previous studies to characterize the crystalline silica aerosol from cutting fiber-cement.[43,44] In this study, aerosol was generated in the test chamber by manually grinding a stack of the engineered stone samples using a hand-held pneumatic angle grinder (GPW-216, Gison Machinery Co., Ltd., Taiwan) equipped with a 10 cm diameter, coarse, diamond grinding cup wheel (Model SIS-4SPCW-SC, Stone Industrial Supplies, Inc., USA). A demonstration video of the grinding process is available in the SI. Each test consisted of three cycles comprised of 4 min of grinding followed by 1 min idling time (a total of 12 min of active grinding time and 3 min idling time). A total of six tests were conducted as detailed in Table 1. The aerosol was carried downstream to a measurement duct at a controlled and constant airflow velocity of about 2.26 m/s corresponding to a flow velocity of 0.11 m/s in the chamber in accordance with the European Standard EN 1093−3.[42] The measurement duct contained near-isokinetic sampling probes for sampling and monitoring the aerosol. The sampling bias from these probes was estimated to be <10% for particles smaller than 19 μm.[28] The number size distribution of the aerosol was measured by an Aerodynamic Particle Sizer (APS) Spectrometer (Model 3321, TSI Inc.). Size fractionated aerosol was collected using a Micro-Orifice Uniform-Deposit Impactor (MOUDI) (Model 110-R, TSI Inc.) that consists of different stages with cut sizes (d_{50}) of 18 μm (precut), 10 μm, 5.6 μm, 3.2 μm, 1.8 μm, 1.0 μm, 0.56 μm, 0.32 μm, 0.18 μm, 0.10 μm, 0.056 μm, and <0.056 μm (after filter), at a flow rate

https://doi.org/10.1021/acsomega.4c06437
ACS Omega 2024, 9, 50308−50317

of 30 lpm. The MOUDI's air flow rate was calibrated by a mass flow meter (Model 4043H, TSI Inc.) before each use. The pressure drop in the MOUDI remained consistent before and during measurements. The impactor nozzles were cleaned using 2-propanol (reagent grade, TSI Inc.) after each test.

Size fractionated calibration samples for XRD/FT-IR were collected using the MOUDI and the Quartz Crystal Microbalance MOUDI (QCM MOUDI, TSI Inc.) as detailed in Table 1. The QCM MOUDI consists of six stages with d_{50} of 0.960 μm, 0.510 μm, 0.305 μm, 0.156 μm, 0.074 and 0.045 μm at a flow rate of 10 lpm. For FT-IR calibration, additional size-fractionated Min-U-Sil 5 samples with aerodynamic diameters of 0.32 μm, 0.56 μm, and 1 μm were obtained independently using the Aerodynamic Aerosol Classifier (AAC; Cambustion Ltd., Cambridge, United Kingdom) and NanoSpot Collector (Aerosol Devices Inc., Fort Collins, CO) as detailed in Table 1. The NanoSpot Collector concentrated the sampled aerosol on a small spot for enhanced analytical measurement sensitivity over a shorter sampling time.[45] All filters were conditioned in a humidity-controlled chamber prior to weighing. All gravimetric measurements were performed on an ultramicro balance (Model XPR6U, Mettler-Toledo). Each filter was pre- and post-weighed thrice and the difference of the averages was the representative mass of the aerosol/calibration material.

2.3. Sample Analysis Methods. *X-ray Diffraction (XRD) Measurements.* The silver filters with aerosol/calibration samples were mounted onto holders atop a "zero background" backing plate made of silicon single crystal. The crystalline silica content in the size-fractionated aerosol samples was measured using an X-ray diffractometer (Empyrean series 2, PANalytical, The Netherlands). The diffractometer was equipped with a 1.8 kW long fine focus Cu X-ray tube operated at 45 kV and 40 mV, 0.04 rad Soller slit, 10 mm mask, 2° antiscatter slit and 1/2° divergence slit, Bragg–Brentano HD, and PIXcel 3D detector. XRD measurements were conducted over a 2θ-range from 20° to 40° with 0.02° step size for each sample. During XRD batch measurements, an instrument reference standard (PANalytical, The Netherlands) was analyzed to account for long-term tube drift. The peak intensity of this standard was used as a correction factor following the NIOSH 7500 method.[47] The calibration curves for quartz and cristobalite were obtained by plotting the net height of each primary peak (located at 26.69° 2θ and 22.02° 2θ for quartz and cristobalite, respectively) as a function of the reference material mass on the filter for each size-fractionated sample. The slope from each size-fractionated calibration curve was compared to the mass normalized net XRD peak height from the aerosol samples to quantify the fractional quartz and cristobalite contents.

Fourier Transform Infrared (FT-IR) Spectroscopy Measurements. The PVC filters with aerosol/calibration samples were mounted on FT-IR sample cards (International Crystal Laboratories, Garfield, NJ). The absorbance was measured using an FT-IR spectrometer (Alpha-II, universal sample model, Bruker) with a spectral range of 400–4000 cm^{-1} at 2 cm^{-1} resolution. For each sample, the absorption spectrum (averaged over 16 scans) was obtained three times. Since the characteristic FT-IR vibration mode from both silica polymorphs interfere with each other at 800 cm^{-1} (normally used to quantify the crystalline silica content), distinct signature peaks for quartz and cristobalite according to NIOSH Method 7602 were selected for analysis.[49] The quartz and cristobalite peak heights of the absorbance band at 695 cm^{-1} (baseline between 680 and 710 cm^{-1}) and 625 cm^{-1} (baseline between 610 and 630 cm^{-1}), respectively, were measured. Like the XRD method, size-fractionated calibration curves were prepared and used to determine the quartz/cristobalite content in different size fractions of the aerosol.

Electron Microscopy. For multiparticle characterization, a Phenom XL (Thermo Fisher Scientific, Waltham, MA, USA) scanning electron microscope (SEM) operated in the low-pressure mode (~1 Pa) at 15 kV acceleration voltage and 1.7 nA probe current with a backscattered electron (BSE) detector and an energy dispersive X-ray spectrometer (EDS) was used. To characterize individual particles at high magnifications, we used a JEOL 2100F (JEOL USA, Peabody, MA) scanning transmission electron microscope (STEM) with a field emission gun, equipped with an EDS detector (X-Max80T, Oxford Instruments America, Concord, MA) and a post-column Gatan Image Filter (GIF) (Tridiem 863, Gatan, Pleasanton, CA). Composition, crystallinity, and local electronic structure of individual silica particles in the samples were examined by EDS, selected area electron diffraction (SAED), and electron energy loss structure (EELS), respectively.

Optical Photothermal Infrared (O-PTIR) Spectroscopy. An advanced optical photothermal infrared (O-PTIR) spectroscopy microscope (Photothermal Spectroscopy Corp., Santa Barbara, CA) was used to detect the presence of polymeric resin in the sub-100 nm and respirable size fractions of the aerosol. The O-PTIR microscope is equipped with a tunable mid-IR quantum-cascade laser (QCL) source (Block Engineering, Southborough, MA) and a 532 nm laser, both collimated through an 40X/0.78N.A. reflective objective (PIKE Technologies, Inc., Madison, WI). O-PTIR spectra were recorded at increments of 0.1 μm along both coplanar axes from a 5 μm × 2.7 μm region on the filter sample (see footnote j in Table 1) in the wavenumber range of 771–1881 cm^{-1} at a resolution of 2 cm^{-1}.

3. RESULTS AND DISCUSSION

3.1. Calibration for XRD and FT-IR Measurements. The engineered stone studied in this work contains two crystalline silica polymorphs, i.e., quartz and cristobalite, which are known to be Group 1 carcinogens to humans.[50] Raman and XRD characterization confirmed the presence of both polymorphs in the bulk engineered stone; the details of this characterization is presented in Figure S2 in the SI.

The mass-weighted size distribution measured using the MOUDI for the aerosol from grinding operation was compared with the quartz (Min-U-Sil 5) and cristobalite (SRM 1879b) reference materials in Figure S3 in the SI. The modal diameter of the aerosol from grinding was 75% higher than these two standards, which required using size-fractionated calibrations. While the infrared absorption does depend on the particle sizes according to the Lorenz-Mie theory,[51] the attenuation of X-ray diffracted intensity in powder samples occurs at particle diameters much greater than those studied in this work. The apparent reduction in X-ray diffracted intensity with decreasing particle size has been attributed by the previous studies to a disordered, amorphous layer on the particle surface formed during comminution,[52−54] and can account for several percent of the total particulate mass in finely divided solids according to the SRM certification.[55,56] However, we surmise that the drop in the diffracted intensity observed at smaller particle size (≪ 1 μm)

https://doi.org/10.1021/acsomega.4c06437
ACS Omega 2024, 9, 50308−50317

is likely due to many factors, including: (i) increased relative abundance of amorphous silica content (either due to amorphous particles or as a surface amorphous layer on crystalline particles as noted above), (ii) loss of smaller particles to the deeper filter matrix during sample preparation, which are in the "shadow" and not effectively available for X-ray diffraction analysis[57] (thereby reducing the net particulate mass probed by the X-ray beam relative to gravimetric mass of total particulate sample), and (iii) the loss of particles during sample preparation (for example, during plasma ashing and redeposition), the magnitude of which is strongly dependent on the particle size. Employing a size-fractionated calibration curve used in this study accounts and corrects for artifacts related to the factors mentioned in (ii) and (iii) above. In order to minimize the artifacts associated with the factor noted in (i) above, it is essential to construct calibration curves using a reference material that has the highest crystalline phase purity (close to 100%).

Mass-normalized XRD height (left-axis) from the primary peak of the quartz reference materials as a function of d_{50} as shown in Figure 1(a) was used for calibration. The normalized peak height decreased steadily with decreasing particle diameter below 10 μm, reducing by 50% for d_{50} of 1 μm and by an order of magnitude (about 90%) for particles in the sub-100 nm range. The normalized peak height of the SRM 1878 particles on stage 1 of QCM (d_{50} of 0.96 μm) and Min-U-Sil 5 particles on stage 5 of MOUDI (d_{50} of 1.0 μm) were similar, indicating that the independent measurements by different cascade impactors were consistent. Our size-fractionated calibration curve for XRD agreed with literature studies within the range of uncertainties that are typical for such measurements.[52,57−59] Due to differences in the diffractometers used in these studies, the relative normalized peak height (right-axis) expressed as a percentage was plotted as a function of aerodynamic size in Figure 1(a). Projected area diameter from microscopy[52] and spherical equivalent diameter[57] were converted to aerodynamic diameter after accounting for the dynamic shape factor (1.36), density (2.65 g/cm^3), and slip correction factor (<1.08 for particle size >1 μm).[60] The size-fractionated XRD calibration curve for cristobalite reference material is shown Figure S4(a) in the SI.

Similarly, the mass-normalized FT-IR peak height (left-axis) from the 695 cm^{-1} peaks of the quartz reference materials (Min-U-Sil 5 and SRM 1878b) as a function of $d_{50,}$ shown in Figure 1(b), was used for calibration. Unlike XRD, the normalized peak height generally decreased with an increasing particle diameter up to 1.8 μm. Beyond this, a maximum was observed at 3.2 μm following which the FT-IR signal decreased. The normalized FT-IR signal for three size-fractionated samples with aerodynamic diameters of 0.32 μm, 0.56 μm, and 1 μm using the AAC were also in agreement with the MOUDI. Our size-fractionated calibration curve for FT-IR agreed with literature studies.[61−65] For comparison, the relative normalized peak height (right-axis) expressed as a percentage was plotted as a function of aerodynamic size in Figure 1(b). Here again, the projected area diameter[61] and the spherical equivalent diameters,[62−64] were converted to the aerodynamic diameters. A similar FT-IR calibration curve for the cristobalite reference material is shown in Figure S4(b) in the SI.

3.2. Fractional Silica Content in Sub-100 nm Fraction.

The quartz and cristobalite mass content (%) for the size-fractionated aerosol quantified through XRD and FT-IR calibrations are shown in Figure 2(a) and (b), respectively.

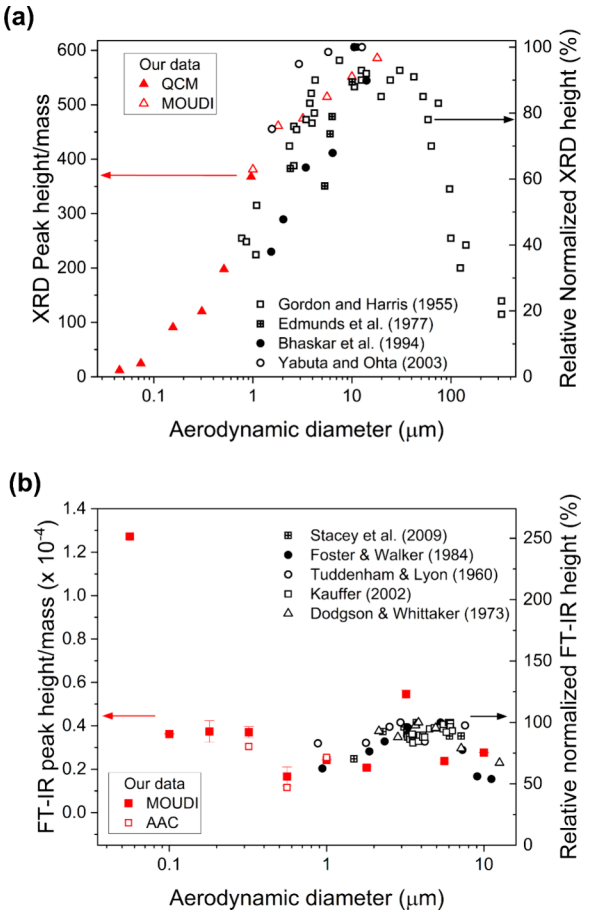

Figure 1. Calibration curves for quartz using (a) XRD and (b) FT-IR spectroscopy. (a) XRD peak height was normalized by quartz mass (left-axis) for SRM 1878 and Min-U-Sil 5 standards which were size-fractionated using QCM and MOUDI impactors, respectively. Literature data[52,57−59] was compared by plotting the relative normalized XRD height (right-axis). (b) FT-IR peak heights normalized by quartz mass for Min-U-Sil 5 and SRM 1878b standards size-fractionated using MOUDI. The error bars for MOUDI represent one standard deviation of replicate samples as detailed in Table 1. Literature data[61−65] was compared by plotting the relative normalized FT-IR height (right-axis).

We performed a nonparametric statistical test (Kruskal−Wallis ANOVA) on our data across all size fractions and found no significant difference between the quartz content, while the cristobalite content was significantly different. The results of the Kruskal−Wallis ANOVA are detailed in Table S1 in the SI. The results in Figure 2(b) indicate that the cristobalite content in the aerosol particles increased from about 10−20% in the sub-100 nm range to 40−50% in the respirable size range. The reasons for this observation are not known and need further investigation. The crystalline silica quantification from the XRD method was within the measurement uncertainty of the FT-IR method for most size fractions. However, the significant deviation observed for some FT-IR measurements compared to XRD could likely be attributed to spectral interference from other minerals in the engineered stone (elemental analysis presented in the next section showed the presence of several other inorganic components). For example, if present in the matrix, the characteristic FT-IR vibration bands for calcium carbonate (700 cm^{-1})[66] and sodium oxide (696 cm^{-1})[67] could interfere with the quartz quantification. Similarly, the broad

https://doi.org/10.1021/acsomega.4c06437
ACS Omega 2024, 9, 50308−50317

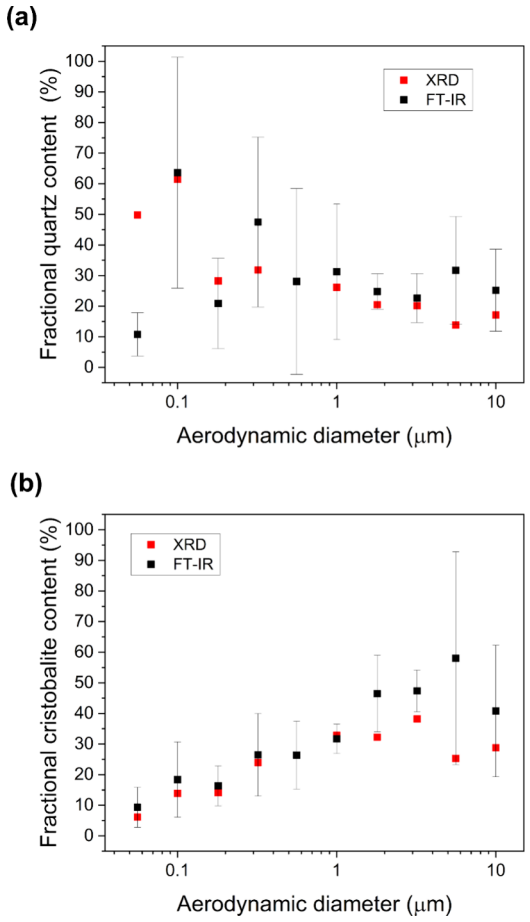

Figure 2. Crystalline silica mass content for (a) quartz, and (b) cristobalite, using XRD and FT-IR methods for size-fractionated engineered stone samples. The error bars for FT-IR quantifications represent the measurement uncertainty in estimating the fractional crystalline silica content from the four replicate samples (See Table 1).

FT-IR peaks for alumina (635 cm^{-1})[68] and iron oxide (610 cm^{-1})[69] could interfere with the cristobalite quantification. The large measurement uncertainty in FT-IR measurements could be attributed to chemical heterogeneity in the engineered stone, variability in aerosol emission during manual grinding and those associated with aerosol transport and collection in MOUDI.

The total crystalline silica content (quartz + cristobalite) from XRD method in the sub-100 nm size fraction was approximately 55−75%, while it ranged from 40−60% in the respirable size fraction (see Figure S5 in the SI). It is possible that for homogeneous engineered stone materials, the fractional crystalline silica content may not vary significantly as a function of particle size; however, the fractional crystalline silica content could vary substantially across different particle size ranges if the bulk material is heterogeneous. Furthermore, fractioning of crystalline silica in various particle size ranges can also depend on the nature of stone grinding, cutting, or fabrication mechanism. Figure S5 in the SI shows that the conventional calibration[47] (as opposed to the size-fractionated calibration approach) underestimates the crystalline silica content in the submicron size fraction for XRD. No clear trend was observed when comparing the crystalline silica content between the conventional and size-fractionated FT-IR calibrations in Figure S5 in the SI. Although, the total crystalline silica content from the size fractionated FT-IR calibration (see Figure S5 in the SI) is in reasonable agreement with the size-fractionated XRD calibration for most size fractions, caution must be exercised while using the FT-IR method due to the higher uncertainty in both sub-100 nm and respirable size fractions.

3.3. Confirmatory Analysis to Support XRD/FT-IR Quantifications. The elemental composition of the particles across all size-fractionated samples was investigated using SEM/EDS. Figure 3(a)-(h) shows the images of aerosol collected on MOUDI stages 0 through 7 (magnified from the SEM micrographs in Figure S6 in the SI). The particles appeared to be compact with sharp fractured edges possibly due to the grinding operation. Spot analysis on multiple particles on each stage revealed an abundance of Si and O, which could be attributed to either crystalline or amorphous silica (SiO_2) in the engineered stone. Figure 3(i) and (j) show the STEM dark field images and corresponding EDS elemental maps of particles collected on impactor stages 8 and 9, respectively. The detection of Ti could be attributed to the presence of titania (TiO_2) pigment, whereas Ca, Cr, and Mo could indicate the presence of calcite, chromite, and molybdenite, respectively, in the engineered stone and is consistent with earlier studies.[70,71] Existence of elemental Ca, Al, Na, and Fe suggests possible presence of other inorganic oxides in the engineered stone that could potentially lead to FT-IR spectral interference and higher uncertainties associated with crystalline silica quantification as discussed in the preceding section. With the exception of calcite which may show minor interference at 26.69° 2θ in quartz quantification, no peak interference in XRD quantifications is expected due to the presence of these inorganic oxides.[68]

Figure 4 shows hyperspectral images of respirable particles (stage 4) and sub-100 nm particles (stage 9) and the corresponding average FT-IR spectrum from the mapped area. The red regions correspond to maximum intensity of the 1720 cm^{-1} peak associated with C = O from polyester resin, whereas the yellow regions correspond to the 800 cm^{-1} peak associated with Si−O−Si from crystalline or amorphous silica. The lack of red regions in the hyperspectral image from the stage 9 sample indicated that the sub-100 nm aerosol was deficient in resin particles. Moreover, the 1720 cm^{-1} peak was not observed for the submicron particles (stages 7 through 10) in the FT-IR spectra (see Figure S7 in SI) as well. However, the presence of the 1720 cm^{-1} peaks on the stage 4 sample in Figure 4 and Figure S7 in SI indicated that the resin particles were limited to the respirable size range. This could explain the slightly lower fractional crystalline silica content in the respirable size fraction as compared to the sub-100 nm size fraction in Figure S5 in the SI.

SAED patterns were used to distinguish between crystalline and amorphous silica phases in individual particles. Figure 5(a) shows the TEM image of a particle with lateral size of about 68 nm from stage 9 of the MOUDI. The electron diffraction pattern of this particle showed bright spots confirming the particle's crystallinity as shown in the inset of Figure 5(a). This sub-100 nm particle contained elemental Si and O based on EDS analysis (spectra not shown). A TEM image of a respirable particle with lateral size of about 1.9 μm from stage 4 of the MOUDI in Figure 5(b) was confirmed to be silica through EDS mapping (Figure S8(a) in SI). The presence of crystalline regions within this specific particle was confirmed

https://doi.org/10.1021/acsomega.4c06437
ACS Omega 2024, 9, 50308−50317

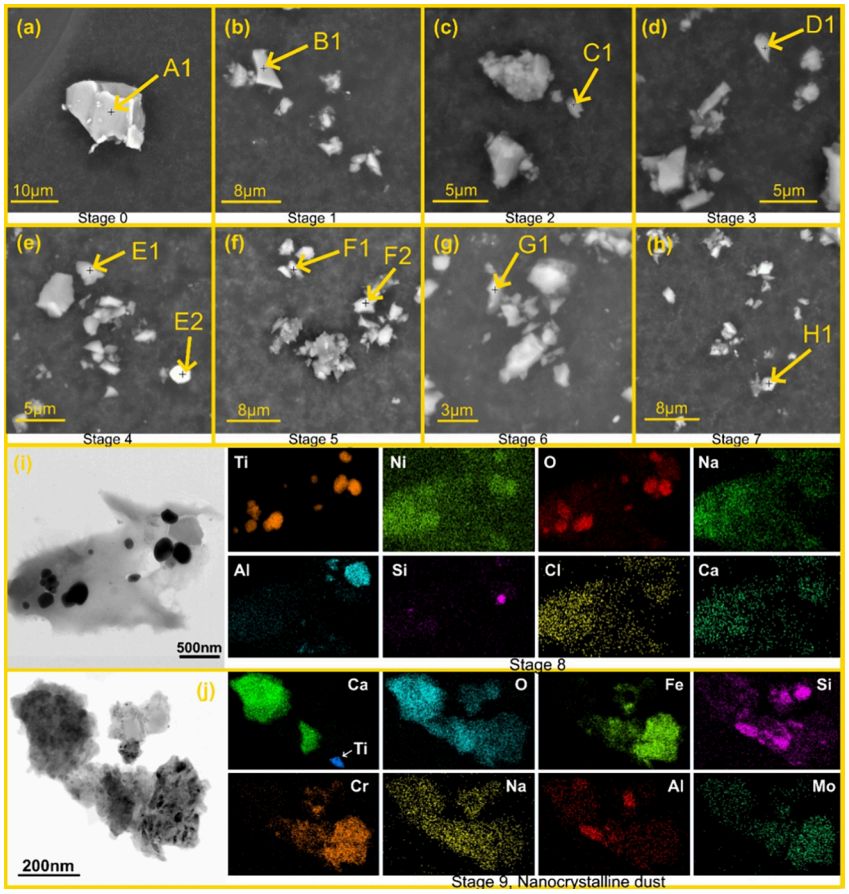

Figure 3. (a)-(h) SEM micrographs and EDS elemental analysis for aerosol particles from grinding of engineered stone collected on MOUDI stages 0 through 7. Composition of particles marked in the images is summarized in Table S2 in the SI. All other particles were identified as silica. (i)-(j) STEM micrographs and EDS analysis for MOUDI stages 8 and 9. The presence of Si, O, Al, Na, Fe, and Ti elements indicate that the released particles contained predominantly crystalline/amorphous silica, and a fraction of metal oxides of Al, Na, Fe, and Ti.

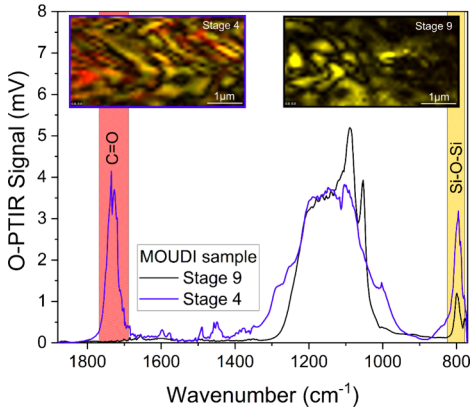

Figure 4. Hyperspectral images of aerosols from the griding of engineered stone collected on stage 4 and stage 9 of the MOUDI. The yellow regions indicate the maximum intensity from the 800 cm^{-1} vibration mode for crystalline silica, whereas the red regions indicate the maximum intensity from the 1720 cm^{-1} vibration mode for polyester (from the resin matrix of engineered stone). The orange regions indicate an overlap of the two vibration modes.

through electron diffraction patterns recorded at the center (location 1) and edge (location 2) as shown in Figure 5(b). However, the electron diffraction pattern on the outer edge (location 3) displayed concentric rings attributed to the amorphous halo indicative of the lack of crystalline order. The existence of this amorphous region along the particle's periphery was further confirmed through EELS line scan recorded in the blue encircled region in Figure 5(b). Details of this characterization are presented in Figure S8(c)-(e) in the SI. This amorphous layer in quartz particles has been attributed to mechanical processing.[53] In contrast, the three edges (locations 1, 2, and 3) of a submicron silica particle from stage 8 of the MOUDI shown in Figure S8(b) in the SI were determined to be crystalline, like the center (location 4), based on the electron diffraction patterns. Whether the degree of crystallinity of the sub-100 nm and submicron silica particles impacts their potential toxicity compared to the respirable silica particles deserves further investigation.

4. LUNG DEPOSITED MASS AND SURFACE AREA

To further probe the deposited dose in terms of different metrics, the worker exposure to crystalline silica in the aerosol from grinding of the engineered stone ($dM/dLogd_p$ vs d_{50} from MOUDI multiplied by the total crystalline silica based on both conventional and size-fractionated XRD calibrations in Figure S5) was multiplied by the respirable fraction defined per the American Conference of Governmental Industrial Hygienists (ACGIH) criterion[60] and the respiratory deposition fraction based on the International Commission on Radiological Protection (ICRP) deposition model.[72] Figure 6 shows the cumulative distribution of lung deposited crystalline silica from grinding. These calculations provide a crude estimate of

https://doi.org/10.1021/acsomega.4c06437
ACS Omega 2024, 9, 50308−50317

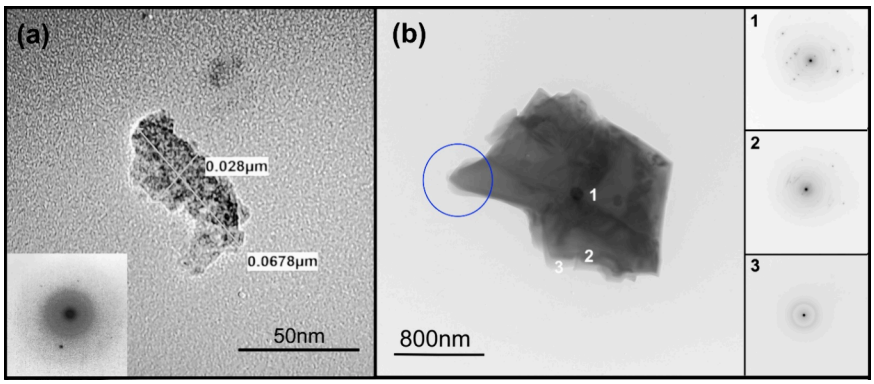

Figure 5. (a) TEM image with electron diffraction pattern of a sub-100 nm crystalline silica particle from stage 9 of the MOUDI; (b) TEM image of a respirable aerosol particle from stage 4 of the MOUDI. Electron diffraction patterns from locations 1, 2, and 3 on the particle. The SAED images shown here were inverted in color to resolve the bright diffraction spots. EELS spectra characterized in Figure S8(c)-(e) in the SI were obtained from the encircled blue region.

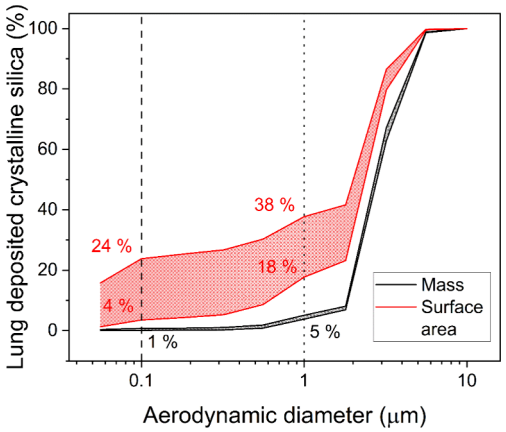

Figure 6. Cumulative distribution of the lung deposited crystalline silica in the aerosol from grinding based on mass- and surface area. The percentages indicated for each distribution represent the contribution of the sub-100 nm and submicron fractions to the total aerosol deposited in the lung. The shaded region between upper and lower curves represents range of values obtained from both conventional (lower bound) as well as size-fractionated (upper bound) XRD calibration curves.

surface area associated with crystalline silica, since the approach assumes that the entire crystalline silica mass (in each size range) is composed of particles that are spherical and are made of crystalline silica, which may not be the case for the engineered stone aerosols. Based on mass, the submicron fraction contributed to about 5% of the crystalline silica deposition, whereas the sub-100 nm fraction contributed to only about 1%.

Studies have demonstrated surface area to be a more relevant metric for assessing particle toxicity.[73−78] Some studies on crystalline silica aerosol also suggest the importance of surface area in influencing silica toxicity.[79−82] Freshly fractured crystalline silica has been shown to induce AP-1 activation four times higher than aged silica in JB6 cells and generate more reactive oxygen species when incubated with cells.[79] The toxicological effects of crystalline silica exposure have been attributed to the presence of conchoidal fractures on the surface which lead to the generation of surface radicals[80] and impact the spatial arrangement of the surface silanols and siloxanes.[81,82] A straightforward conversion of $dM/dLogd_p$ using the specific surface area of each particle with diameter d_{50} was used to compute $dS/dLogd_p$. Based on this surface area metric, approximately 4−24% and 18−38% of the crystalline silica deposited in the lung is attributed to the sub-100 nm and submicron fractions, respectively. If the surface area is a more relevant exposure metric for crystalline silica particles, the assessment of efficacy of current engineering control systems using mass as an exposure metric may not provide adequate protection for NCS as well as RCS fractions.

5. CONCLUSIONS

The size-resolved fractional silica content of NCS and RCS released during grinding of an engineered stone material in laboratory test chamber experiments was investigated and quantified by the XRD and FT-IR analysis, showing the presence of both α-quartz (15−60%) and cristobalite (10−50%) polymorphs in NCS and RCS. The combination of cristobalite and α-quartz was found to make up more than 70% of the total mass in the sub-100 nm fraction, while no polymeric resin binder was detected. Conventional calibration based on polydisperse standards may underestimate the crystalline silica content in the submicron size range compared to that obtained using the size-fractionated calibration for XRD. Quantification of crystalline silica using FT-IR in aerosols from engineered stone can result in larger uncertainty due to interference from other inorganic oxides.

This study demonstrates the potential of submicron RCS exposure during grinding of engineered stone countertop materials. Only one engineered stone sample was tested in this study and the results cannot be generalized to all stone countertops because of variability in stone characteristics, fabrication operations, and the particle size distribution of dust generated.

■ ASSOCIATED CONTENT

Data Availability Statement

The data underlying this study are available in the published article and its Supporting Information. Additional data are available from the corresponding author on reasonable request.

Supporting Information

The Supporting Information is available free of charge at https://pubs.acs.org/doi/10.1021/acsomega.4c06437.

Details about the experimental setup chamber, XRD and Raman analysis of bulk powder from the engineered stone, mass-weighted size distributions of the aerosol

https://doi.org/10.1021/acsomega.4c06437
ACS Omega 2024, 9, 50308−50317

from grinding engineered stone, XRD/IR size-fractionated calibration curves for cristobalite (SRM 1879b), comparison of total crystalline silica content based on size-fractionated and conventional calibration, SEM micrographs of size fractionated aerosol dust, FT-IR spectra for size fractionated aerosol samples, and EDS/electron diffraction/EELS spectra of respirable aerosol particle (PDF)

Video of stone grinding in the chamber (MP4)

AUTHOR INFORMATION

Corresponding Author

Bon Ki Ku − *Health Effects Laboratory Division (HELD), National Institute for Occupational Safety and Health (NIOSH) Centers for Disease Control and Prevention (CDC), Cincinnati, Ohio 45226, United States;* orcid.org/0000-0002-1233-0790; Phone: +1 513 841 4147; Email: bku@cdc.gov; Fax: +1 513 841 4545

Authors

Kabir Rishi − *Health Effects Laboratory Division (HELD), National Institute for Occupational Safety and Health (NIOSH) Centers for Disease Control and Prevention (CDC), Cincinnati, Ohio 45226, United States;* orcid.org/0000-0002-3159-031X

Chaolong Qi − *Division of Field Studies and Engineering (DFSE), National Institute for Occupational Safety and Health (NIOSH) Centers for Disease Control and Prevention (CDC), Cincinnati, Ohio 45226, United States*

Drew Thompson − *Division of Field Studies and Engineering (DFSE), National Institute for Occupational Safety and Health (NIOSH) Centers for Disease Control and Prevention (CDC), Cincinnati, Ohio 45226, United States;* orcid.org/0000-0003-4011-3619

Chen Wang − *Health Effects Laboratory Division (HELD), National Institute for Occupational Safety and Health (NIOSH) Centers for Disease Control and Prevention (CDC), Cincinnati, Ohio 45226, United States;* orcid.org/0000-0002-2343-339X

Alan Dozier − *Health Effects Laboratory Division (HELD), National Institute for Occupational Safety and Health (NIOSH) Centers for Disease Control and Prevention (CDC), Cincinnati, Ohio 45226, United States*

Vasileia Vogiazi − *Health Effects Laboratory Division (HELD), National Institute for Occupational Safety and Health (NIOSH) Centers for Disease Control and Prevention (CDC), Cincinnati, Ohio 45226, United States*

Orthodoxia Zervaki − *Health Effects Laboratory Division (HELD), National Institute for Occupational Safety and Health (NIOSH) Centers for Disease Control and Prevention (CDC), Cincinnati, Ohio 45226, United States;* orcid.org/0000-0002-3481-506X

Pramod Kulkarni − *Health Effects Laboratory Division (HELD), National Institute for Occupational Safety and Health (NIOSH) Centers for Disease Control and Prevention (CDC), Cincinnati, Ohio 45226, United States*

Complete contact information is available at: https://pubs.acs.org/10.1021/acsomega.4c06437

Author Contributions

Kabir Rishi: conceptualization, data curation, formal analysis, investigation, methodology, validation, visualization, writing−original draft preparation, writing−reviewing and editing. Bon Ki Ku (corresponding author): funding acquisition, methodology, project administration, resources, formal analysis, investigation, writing−reviewing and editing. Chaolong Qi: investigation, writing−reviewing. Drew Thompson: investigation, writing−reviewing. Chen Wang: investigation. Alan Dozier: investigation. Vasileia Vogiazi: investigation. Orthodoxia Zervaki: investigation. Pramod Kulkarni: conceptualization, writing−reviewing.

Funding

This work was funded by the National Institute for Occupational Safety and Health through the Nanotechnology Research Center (NTRC) program (CAN 9390DTE and CAN 9390MAC).

Notes

The findings and conclusions in this report are those of the author(s) and do not necessarily represent the official position of the National Institute for Occupational Safety and Health, Centers for Disease Control and Prevention. The mention of any company or product does not constitute an endorsement by the Centers for Disease Control and Prevention.

The authors declare no competing financial interest.

Activity was determined to meet the definition of research as defined in 46.102(l) but did not involve human subjects as defined in 46.103(e)(1).

ACKNOWLEDGMENTS

The authors would like to thank Dr. Aleks Stefaniak at the Respiratory Health Division (RHD), NIOSH for reviewing the manuscript and providing critical feedback. We would like to thank U.S. Silica Company (Katy, TX) for providing Min-U-Sil 5 powder at no cost.

REFERENCES

(1) Glindmeyer, H. W.; Hammad, Y. Y. Contributing Factors to Sandblasters' Silicosis: Inadequate Respiratory Protection Equipment and Standards. *J. Occup. Environ. Med.* **1988**, *30* (12), 917−921.

(2) Thorpe, A.; Ritchie, A. S.; Gibson, M. J.; Brown, R. C. Measurements of the Effectiveness of Dust Control on Cut-off Saws Used in the Construction Industry. *Ann. Occup. Hyg.* **1999**, *43* (7), 443−456.

(3) Nash, N. T.; Williams, D. R. Occupational Exposure to Crystalline Silica During Tuckpointing and the Use of Engineering Controls. *Appl. Occup. Environ. Hyg.* **2000**, *15* (1), 8−10.

(4) Akbar-Khanzadeh, F.; Brillhart, R. L. Respirable Crystalline Silica Dust Exposure During Concrete Finishing (Grinding) Using Hand-Held Grinders in the Construction Industry. *Ann. Occup. Hyg.* **2002**, *46* (3), 341−346.

(5) Linch, K. D. Respirable Concrete Dust–Silicosis Hazard in the Construction Industry. *Appl. Occup. Environ. Hyg.* **2002**, *17* (3), 209−221.

(6) Rappaport, S. M.; Goldberg, M.; Susi, P.; Herrick, R. F. Excessive Exposure to Silica in the US Construction Industry. *Ann. Occup. Hyg.* **2003**, *47* (2), 111−122.

(7) Heinzerling, A.; Cummings, K. J.; Flattery, J.; Weinberg, J. L.; Materna, B.; Harrison, R. Radiographic Screening Reveals High Burden of Silicosis among Workers at an Engineered Stone Countertop Fabrication Facility in California. *Am. J. Respir. Crit. Care Med.* **2021**, *203* (6), 764−766.

(8) Rose, C.; Heinzerling, A.; Patel, K.; Sack, C.; Wolff, J.; Zell-Baran, L.; Weissman, D.; Hall, E.; Sooriash, R.; McCarthy, R. B.; Bojes, H.; Korotzer, B.; Flattery, J.; Weinberg, J. L.; Potocko, J.; Jones, K. D.; Reeb-Whitaker, C. K.; Reul, N. K.; LaSee, C. R.; Materna, B. L.; Raghu, G.; Harrison, R. Severe Silicosis in Engineered Stone Fabrication Workers — California, Colorado, Texas, and Washington,

2017−2019. *MMWR. Morb. Mortal. Wkly. Rep.* **2019**, *68* (38), 813−818.
(9) Dodd, K.; Heinzerling, A.; Rose, C.; Reeb-Whitaker, C.; Harrison, R. *Outbreak of Silicosis among Engineered Stone Countertop Workers in Four States* https://blogs.cdc.gov/niosh-science-blog/2019/10/29/silicosis-countertop/.
(10) Worthington, K.; Filios, M.; Reilly, M. J.; Harrison, R.; Rosenman, K. D. *Silica Hazards from Engineered Stone Countertops* https://blogs.cdc.gov/niosh-science-blog/2014/03/11/countertops/.
(11) OSHA−2010−0034. Occupational Exposure to Respirable Crystalline Silica, Final Rule. *Fed. Regist.* **2016**, *81* (58), 16826−16890.
(12) NIOSH. Work-Related Lung Disease (WoRLD) Surveillance Report 2007. DHHS (NIOSH) Publication No. 2008-143. http://www.cdc.gov/niosh/docs/2008-143/.
(13) Requena-Mullor, M.; Alarcón-Rodríguez, R.; Parrón-Carreño, T.; Martínez-López, J. J.; Lozano-Paniagua, D.; Hernández, A. F. Association between Crystalline Silica Dust Exposure and Silicosis Development in Artificial Stone Workers. *Int. J. Environ. Res. Public Health* **2021**, *18* (11), 5625.
(14) WorkCover Queensland. *1000+ stonemasons now screened for silicosis in Queensland* https://www.worksafe.qld.gov.au/news-and-events/newsletters/esafe-newsletters/esafe-editions/esafe/february-2020/1000-stonemasons-now-screened-for-silicosis-in-queensland.
(15) Leso, V.; Fontana, L.; Romano, R.; Gervetti, P.; Iavicoli, I. Artificial Stone Associated Silicosis: A Systematic Review. *Int. J. Environ. Res. Public Health* **2019**, *16* (4), 568.
(16) Kirby, T. Australia Reports on Audit of Silicosis for Stonecutters. *Lancet* **2019**, *393* (10174), 861.
(17) Hoy, R. F.; Baird, T.; Hammerschlag, G.; Hart, D.; Johnson, A. R.; King, P.; Putt, M.; Yates, D. H. Artificial Stone-Associated Silicosis: A Rapidly Emerging Occupational Lung Disease. *Occup. Environ. Med.* **2018**, *75* (1), 3−5.
(18) Pérez-Alonso, A.; Córdoba-Doña, J. A.; Millares-Lorenzo, J. L.; Figueroa-Murillo, E.; García-Vadillo, C.; Romero-Morillo, J. Outbreak of Silicosis in Spanish Quartz Conglomerate Workers. *Int. J. Occup. Environ. Health* **2014**, *20* (1), 26−32.
(19) Kramer, M. R.; Blanc, P. D.; Fireman, E.; Amital, A.; Guber, A.; Rhahman, N. A.; Shitrit, D. Artificial Stone Silicosis: Disease Resurgence among Artificial Stone Workers. *Chest* **2012**, *142* (2), 419−424.
(20) Friedman, G. K.; Harrison, R.; Bojes, H.; Worthington, K.; Filios, M. Notes from the Field: Silicosis in a Countertop Fabricator—Texas, 2014. *MMWR Morb. Mortal Wkly Rep.* **2015**, *64*, 129.
(21) Fazio, J. C.; Gandhi, S. A.; Flattery, J.; Heinzerling, A.; Kamangar, N.; Afif, N.; Cummings, K. J.; Harrison, R. J. Silicosis Among Immigrant Engineered Stone (Quartz) Countertop Fabrication Workers in California. *JAMA Int. Med.* **2023**, *183* (9), 991.
(22) Salamon, F.; Martinelli, A.; Vianello, L.; Bizzotto, R.; Gottardo, O.; Guarnieri, G.; Franceschi, A.; Porru, S.; Cena, L.; Carrieri, M. Occupational Exposure to Crystalline Silica in Artificial Stone Processing. *J. Occup. Environ. Hyg.* **2021**, *18* (12), 547−554.
(23) NIOSH. *Field Evaluation of a Mobile Dust Control Booth for Stone Countertop Grinding, In-Depth Field Survey Report for the Houston, TX Field Survey*. By Qi C, Echt A.; EPHB Report No. 2020-DFSE-165; 2019.
(24) NIOSH. *Engineering Control of Silica Dust from Stone Countertop Fabrication and Installation, In-Depth Field Survey Report for the Houston, TX Field Survey*. By Qi C, Echt A. EPHB Report No. 375−11a; 2016.
(25) NIOSH. *Engineering Control of Silica Dust from Stone Countertop Fabrication and Installation, In-Depth Field Survey Report for the Mendota Heights, MN Field Survey*. By Qi C, Lo L. EPHB Report No. 375−12a; 2016.
(26) NIOSH. *Engineering Control of Silica Dust from Stone Countertop Fabrication and Installation − Evaluation of Wetting Methods for Grinding*. By Qi C, Echt A. EPHB Report NO. 2021-DFSE-710; Cincinnati, OH, 2021.
(27) NIOSH. *Characterization of Airborne Dust Generated from the Grinding of Natural and Engineered Stone Products*. By Thompson D, Qi C. EPHB Report NO. 2023-DFSE-1489; 2023.
(28) Thompson, D.; Qi, C. Characterization of the Emissions and Crystalline Silica Content of Airborne Dust Generated from Grinding Natural and Engineered Stones. *Ann. Work Expo. Heal.* **2023**, *67* (2), 266−280.
(29) DHHS (NIOSH) Publication Number 2002−129. *Health Effects of Occupational Exposure to Respirable Crystalline Silica*; 2002.
(30) Borm, P. J. A.; Fowler, P.; Kirkland, D. An Updated Review of the Genotoxicity of Respirable Crystalline Silica. *Part. Fibre Toxicol.* **2018**, *15* (1), 23.
(31) Marques Da Silva, V.; Benjdir, M.; Montagne, P.; Pairon, J.-C.; Lanone, S.; Andujar, P. Pulmonary Toxicity of Silica Linked to Its Micro- or Nanometric Particle Size and Crystal Structure: A Review. *Nanomaterials* **2022**, *12* (14), 2392.
(32) Li, X. Y.; Brown, D.; Smith, S.; MacNee, W.; Donaldson, K. Short-Term Inflammatory Responses Following Intratracheal Instillation of Fine and Ultrafine Carbon Black in Rats. *Inhal. Toxicol.* **1999**, *11* (8), 709−731.
(33) Nemmar, A.; Hoylaerts, M. F.; Hoet, P. H.; Vermylen, J.; Nemery, B. Size Effect of Intratracheally Instilled Particles on Pulmonary Inflammation and Vascular Thrombosis. *Toxicol. Appl. Pharmacol.* **2003**, *186* (1), 38−45.
(34) Zhang, Q.; Kusaka, Y.; Zhu, X.; Sato, K.; Mo, Y.; Kluz, T.; Donaldson, K. Comparative Toxicity of Standard Nickel and Ultrafine Nickel in Lung after Intratracheal Instillation. *J. Occup. Health* **2003**, *45* (1), 23−30.
(35) Warheit, D. B.; Webb, T. R.; Colvin, V. L.; Reed, K. L.; Sayes, C. M. Pulmonary Bioassay Studies with Nanoscale and Fine-Quartz Particles in Rats: Toxicity Is Not Dependent upon Particle Size but on Surface Characteristics. *Toxicol. Sci.* **2007**, *95* (1), 270−280.
(36) Murugadoss, S.; Lison, D.; Godderis, L.; Van Den Brule, S.; Mast, J.; Brassinne, F.; Sebaihi, N.; Hoet, P. H. Toxicology of Silica Nanoparticles: An Update. *Arch. Toxicol.* **2017**, *91* (9), 2967−3010.
(37) Napierska, D.; Thomassen, L. C. J.; Lison, D.; Martens, J. A.; Hoet, P. H. The Nanosilica Hazard: Another Variable Entity. *Part. Fibre Toxicol.* **2010**, *7*, 1−32.
(38) Wang, J. J.; Sanderson, B. J. S.; Wang, H. Cytotoxicity and Genotoxicity of Ultrafine Crystalline SiO2 Particulate in Cultured Human Lymphoblastoid Cells. *Environ. Mol. Mutagen.* **2007**, *48* (2), 151−157.
(39) Ferin, J.; Oberdörster, G.; Soderholm, S. C.; Gelein, R. Pulmonary Tissue Access of Ultrafine Particles. *J. Aerosol Med.* **1991**, *4* (1), 57−68.
(40) Ferin, J.; Oberdörster, G.; Penney, D. P. Pulmonary Retention of Ultrafine and Fine Particles in Rats. *Am. J. Respir. Cell Mol. Biol.* **1992**, *6* (5), 535−542.
(41) Oberdörster, G.; Oberdörster, E.; Oberdörster, J. Nanotoxicology: An Emerging Discipline Evolving from Studies of Ultrafine Particles. *Environ. Health Perspect.* **2005**, *113* (7), 823−839.
(42) CEN. *Safety of Machinery—Evaluation of the Emission of Airborne Hazardous Substances-Part 3: Test Bench Method for Measurement of the Emission Rate for a given Pollutant, EN 1093−3*; CEN: Brussels, Belgium, 2006.
(43) Qi, C.; Echt, A.; Gressel, M. G. On the Characterization of the Generation Rate and Size-Dependent Crystalline Silica Content of the Dust from Cutting Fiber Cement Siding. *Ann. Occup. Hyg.* **2016**, *60* (2), 220−230.
(44) Qi, C.; Echt, A.; Gressel, M. G. The Generation Rate of Respirable Dust from Cutting Fiber Cement Siding Using Different Tools. *Ann. Work Expo. Heal.* **2017**, *61* (2), 218−225.
(45) Zervaki, O.; Stump, B.; Keady, P.; Dionysiou, D. D.; Kulkarni, P. NanoSpot TM Collector for Aerosol Sample Collection for Direct Microscopy and Spectroscopy Analysis. *Aerosol Sci. Technol.* **2023**, *57* (4), 342−354.
(46) Ku, B. K.; Deye, G.; Turkevich, L. A. Characterization of a Vortex Shaking Method for Aerosolizing Fibers. *Aerosol Sci. Technol.* **2013**, *47* (12), 1293−1301.

https://doi.org/10.1021/acsomega.4c06437
ACS Omega 2024, 9, 50308−50317

(47) NIOSH. 7500 - Silica, Crystalline, by XRD (filter redeposition). *NIOSH Manual of Analytical Methods (NMAM)*, 4th ed.; DHHS: Cincinnati, 2003.
(48) NIOSH. 7603 - QUARTZ in Respirable Coal Mine Dust, by IR (Redeposition). *NIOSH Manual of Analytical Methods (NMAM)*, 5th ed.; DHHS: Cincinnati, 2017.
(49) NIOSH. 7602 - SILICA, Respirable Crystalline, by IR (KBrpellet). *NIOSH Manual of Analytical Methods (NMAM)*, 5th ed.; DHHS: Cincinnati, 2017.
(50) Monographs, IARC *on the Identification of Carcinogenic Hazards to Humans. Silica Dust, Crystalline, in the Form of Quartz or Cristobalite; IARC, World Health*; Organization, 2012.
(51) Bohren, C. F.; Huffman, D. R. *Absorption and Scattering of Light by Small Particles*; John Wiley & Sons: New York, US, 2008.
(52) Gordon, R. L.; Harris, G. W. Effect of Particle-Size on the Quantitative Determination of Quartz by X-Ray Diffraction. *Nature* **1955**, *175* (4469), 1135−1135.
(53) Nagelschmidt, G.; Gordon, R. L.; Griffin, O. G. Surface of Finely-Ground Silica. *Nature* **1952**, *169* (4300), 539−540.
(54) Gauthier, R.; Scott, B.; Bennett, J. C.; Salehabadi, M.; Wang, J.; Sainuddin, T.; Obrovac, M. N. The Amorphization of Crystalline Silicon by Ball Milling. *Heliyon* **2024**, *10* (15), No. e34881.
(55) Black, D. R.; Mendenhall, M. H.; Whitfield, P. S.; Windover, D.; Henins, A.; Filliben, J.; Cline, J. P. Certification of Standard Reference Material 1878b Respirable α-Quartz. *Powder Diffr.* **2016**, *31* (3), 211−215.
(56) Black, D. R.; Mendenhall, M. H.; Whitfield, P. S.; Brown, C. M.; Henins, A.; Filliben, J. J.; Cline, J. P. Certification of Standard Reference Material 1879b Respirable Cristobalite. *Powder Diffr.* **2018**, *33* (3), 202−208.
(57) Edmonds, J. W.; Henslee, W. W.; Guerra, R. E. Particle Size Effects in the Determination of Respirable α-Quartz by x-Ray Diffraction. *Anal. Chem.* **1977**, *49* (14), 2196−2203.
(58) Bhaskar, R.; Li, J.; Xu, L. A Comparative Study of Particle Size Dependency of IR and XRD Methods for Quartz Analysis. *Am. Ind. Hyg. Assoc. J.* **1994**, *55* (7), 605−609.
(59) Yabuta, J.; Ohta, H. Determination of Free Silica in Dust Particles: Effect of Particle Size for the X-Ray Diffraction and Phosphoric Acid Methods. *Ind. Health* **2003**, *41* (3), 249−259.
(60) Hinds, W. C. *Aerosol Technology: Properties, Behavior, and Measurement of Airborne Particles*, 2nd ed.; John Wiley & Sons, Inc.: New York, US, 1999.
(61) Tuddenham, W. M.; Lyon, R. J. P. Infrared Techniques in the Identification and Measurement of Minerals. *Anal. Chem.* **1960**, *32* (12), 1630−1634.
(62) Dodgson, J.; Whittaker, W. The Determination of Quartz in Respirable Dust Samples by Infrared Spectrophotometry-I: The Potassium Bromide Disc Method. *Ann. Occup. Hyg.* **1973**, *16* (4), 373−387.
(63) Foster, R. D.; Walker, R. F. Quantitative Determination of Crystalline Silica in Respirable-Size Dust Samples by Infrared Spectrophotometry. *Analyst* **1984**, *109* (9), 1117.
(64) Kauffer, E.; Moulut, J. C.; Masson, A.; Protois, J. C.; Grzebyk, M. Comparison by X-Ray Diffraction and Infrared Spectroscopy of Two Samples of α Quartz with the NIST SRM 1878a α Quartz. *Ann. Occup. Hyg.* **2002**, *46* (4), 409−421.
(65) Stacey, P.; Kauffer, E.; Moulut, J. C.; Dion, C.; Beauparlant, M.; Fernandez, P.; Key-Schwartz, R.; Friede, B.; Wake, D. An International Comparison of the Crystallinity of Calibration Materials for the Analysis of Respirable α-Quartz Using X-Ray Diffraction and a Comparison with Results from the Infrared KBr Disc Method. *Ann. Occup. Hyg.* **2009**, *53* (6), 639−649.
(66) Zhou, G.-T.; Yu, J. C.; Wang, X.-C.; Zhang, L.-Z. Sonochemical Synthesis of Aragonite-Type Calcium Carbonate with Different Morphologies. *New J. Chem.* **2004**, *28* (8), 1027.
(67) *Sodium oxide (1313−59−3) IR1* https://www.chemicalbook.com/SpectrumEN_1313-59-3_IR1.htm (accessed Oct 8, 2023).
(68) Lafuente, B.; Downs, R. T.; Yang, H.; Stone, N. 1. The Power of Databases: The RRUFF Project. In *Highlights in Mineralogical Crystallography*; DE GRUYTER, 2015; pp 1−30. .
(69) NIST Standard Reference Database Number 69. Yellow Iron Oxide Infrared Spectrum. *NIST Chem. Webb.* **2023**. .
(70) Carrieri, M.; Guzzardo, C.; Farcas, D.; Cena, L. G. Characterization of Silica Exposure during Manufacturing of Artificial Stone Countertops. *Int. J. Environ. Res. Public Health* **2020**, *17* (12), 4489−15.
(71) Ramkissoon, C.; Gaskin, S.; Thredgold, L.; Hall, T.; Rowett, S.; Gun, R. Characterisation of Dust Emissions from Machined Engineered Stones to Understand the Hazard for Accelerated Silicosis. *Sci. Rep.* **2022**, *12* (1), 4351.
(72) Smith, H.*Human Respiratory Tract Model for Radiological Protection*; ICRP, Publ. 1994, *66*.
(73) Oberdürster, G. Toxicology of Ultrafine Particles: In Vivo Studies. *Philos. Trans. R. Soc. London. Ser. A Math. Phys. Eng. Sci.* **2000**, *358* (1775), 2719−2740.
(74) Maynard, A. D.; Maynard, R. L. A Derived Association between Ambient Aerosol Surface Area and Excess Mortality Using Historic Time Series Data. *Atmos. Environ.* **2002**, *36* (36−37), 5561−5567.
(75) Lison, D.; Lardot, C.; Huaux, F.; Zanetti, G.; Fubini, B. Influence of Particle Surface Area on the Toxicity of Insoluble Manganese Dioxide Dusts. *Arch. Toxicol.* **1997**, *71* (12), 725−729.
(76) Brown, D. M.; Wilson, M. R.; MacNee, W.; Stone, V.; Donaldson, K. Size-Dependent Proinflammatory Effects of Ultrafine Polystyrene Particles: A Role for Surface Area and Oxidative Stress in the Enhanced Activity of Ultrafines. *Toxicol. Appl. Pharmacol.* **2001**, *175* (3), 191−199.
(77) Dankovic, D.; Kuempel, E.; Wheeler, M. An Approach to Risk Assessment for TiO 2. *Inhal. Toxicol.* **2007**, *19* (sup1), 205−212.
(78) Sager, T. M.; Castranova, V. Surface Area of Particle Administered versus Mass in Determining the Pulmonary Toxicity of Ultrafine and Fine Carbon Black: Comparison to Ultrafine Titanium Dioxide. *Part. Fibre Toxicol.* **2009**, *6* (1), 15.
(79) Ding, M.; Shi, X.; Lu, Y.; Huang, C.; Leonard, S.; Roberts, J.; Antonini, J.; Castranova, V.; Vallyathan, V. Induction of Activator Protein-1 through Reactive Oxygen Species by Crystalline Silica in JB6 Cells. *J. Biol. Chem.* **2001**, *276* (12), 9108−9114.
(80) Fubini, B.; Hubbard, A. Reactive Oxygen Species (ROS) and Reactive Nitrogen Species (RNS) Generation by Silica in Inflammation and Fibrosis. *Free Radic. Biol. Med.* **2003**, *34* (12), 1507−1516.
(81) Turci, F.; Pavan, C.; Leinardi, R.; Tomatis, M.; Pastero, L.; Garry, D.; Anguissola, S.; Lison, D.; Fubini, B. Revisiting the Paradigm of Silica Pathogenicity with Synthetic Quartz Crystals: The Role of Crystallinity and Surface Disorder. *Part. Fibre Toxicol.* **2015**, *13* (1), 1−12.
(82) Pavan, C.; Santalucia, R.; Leinardi, R.; Fabbiani, M.; Yakoub, Y.; Uwambayinema, F.; Ugliengo, P.; Tomatis, M.; Martra, G.; Turci, F.; Lison, D.; Fubini, B. Nearly Free Surface Silanols Are the Critical Molecular Moieties That Initiate the Toxicity of Silica Particles. *Proc. Natl. Acad. Sci. U. S. A.* **2020**, *117* (45), 27836−27846.

https://doi.org/10.1021/acsomega.4c06437
ACS Omega 2024, 9, 50308−50317